

Nonlinear Optical studies of the Transient Coherence in the Quantum Hall System

K.M. Dani^a, E. G. Kavousanaki^b, J. Tignon^c,
 D. S. Chemla^a, and I. E. Perakis^{b,*},

^a *Department of Physics, University of California, Berkeley, and Materials Science Division, Lawrence Berkeley National Laboratory, Berkeley, CA 94720, USA*

^b *Department of Physics, University of Crete, and Institute of Electronic Structure & Laser, Foundation for Research & Technology-Hellas, Heraklion, Crete, Greece*

^c *Laboratoire Pierre Aigrain, Ecole Normale Supérieure, F-75005 Paris, France*

Abstract

We review recent investigations of the femtosecond non-linear optical response of the two-dimensional electron gas (2DEG) in a strong magnetic field. We probe the Quantum Hall (QH) regime for filling factors $\nu \sim 1$. Our focus is on the transient coherence induced via optical excitation and on its time evolution during early femtosecond timescales. We simultaneously study the interband and intraband coherence in this system by using a nonlinear spectroscopic technique, transient three-pulse four wave mixing optical spectroscopy, and a many-body theory. We observe striking differences in the temporal and spectral profile of the nonlinear optical signal between a modulation doped quantum well system (with the 2DEG) and a similar undoped quantum well (without a 2DEG). We attribute these qualitative differences to Coulomb correlations between the photoexcited electron-hole pairs and the 2DEG. We show, in particular, that intraband many-particle coherences assisted by the inter-Landau-level magnetoplasmon excitations of the 2DEG dominate the femtosecond nonlinear optical response. The most striking effect of these exciton-magnetoplasmon coherences is a large off-resonant four-wave-mixing signal in the case of very low photoexcited carrier densities, not observed in the undoped system, with strong temporal oscillations and unusually symmetric temporal profile.

Key words: Quantum Hall Effect, Strong Correlations, Ultrafast Nonlinear Optical Spectroscopy, Collective Effects, Nanostructures

PACS: 71.10.Ca, 71.45.-d, 78.20.Bh, 78.47.+p

* Corresponding author; Tel.: +30-2810-394259

Email address: ilias@physics.uoc.gr (I. E. Perakis).

1 Introduction

The quasiparticle concept is a cornerstone of modern condensed matter physics. The properties of many physical systems can be described, to first approximation, in terms of noninteracting quasiparticles and elementary excitations that may differ substantially from the strongly interacting bare electrons. In many cases, the quasi-static, thermodynamic, linear, and ground state properties do not depend critically on the residual interactions among the quasiparticles. On the other hand, these interactions determine the nonlinear optical dynamics [1,2]. For example, correlations among quasiparticles create quantum coherences in the system, which lead to a new nonlinear optical signal, as well as limit the lifetime of the collective excitations. Such dynamical effects govern the ultrafast nonlinear optical response measured in experiments such as transient wave-mixing and pump-probe [1,3,4,5,6,7,8]. Coherent properties and their manipulation (i.e. coherent control) are central in many areas of physics and chemistry [6,9,10,11,12]. They are currently the subject of intense research due to the many potential applications, e.g. in quantum coherent devices.

In semiconductors, strong correlations and coherences can be mediated by the Coulomb and electron–phonon interactions. These effects are exacerbated in low dimensional nanostructures, where they can even lead to new quantum phases with novel transport and optical properties. An example of such a low dimensional system is the cold two-dimensional electron gas (2DEG) subject to a strong magnetic field perpendicular to the confinement plane [13,14,15,16]. This magnetic field creates discrete Landau levels (LL), which in the ground state are partially filled by electrons introduced by doping. The ratio of occupied states to LL degeneracy gives the filling factor ν . The LL degeneracy increases with magnetic field, and above a threshold value ($\nu \leq 2$), the ground state electrons only occupy the lowest LL (LL0) states; all the higher LLs (LL1, \dots) are then empty in the ground state. The coupling of the degenerate LL states by the Coulomb interaction results in a strongly correlated incompressible quantum liquid with collective charge and spin excitation modes. Examples of such collective excitations that play a central role here are the magnetoplasmon (MP) 2DEG excitations [13,14,15,16,17,18]. The strong exchange Coulomb interactions also stabilize a ground state with spin- \uparrow polarized electron spins for certain integer values of ν or for certain fractional values $\nu = 1/m$, where m is an integer [14]. This paper discusses the crucial role in the transient optical properties of nonequilibrium Coulomb correlations between photoexcited and 2DEG carriers during very early femtosecond time scales.

In addition to creating many-particle coherences and correlations, the interactions among quasiparticles destroy coherence and phase relations within

short time intervals (dephasing or decoherence). By probing the above Quantum Hall (QH) system with very short optical pulses during time scales shorter than its dephasing time, one can observe coherent quantum mechanical effects not accessible with other experiments. In the very early temporal regime, the interactions among quasiparticles should be viewed as quantum mechanical interference phenomena, and well-established pictures, such as the semiclassical Boltzmann picture of dephasing and relaxation, must be revisited [1,2,3,4,6,7]. Indeed, the underlying assumption behind the above approximations is that the duration of the scattering and interaction processes is shorter than the time interval within which we probe the system. However, ultra-short pulses give access to timescales shorter than the characteristic interaction times, determined both by the time it takes for an exciton to dephase and by the time it takes the cold 2DEG to react to the photoexcited excitons (X). The homogeneous dephasing times of the two lowest LL excitons in the QH system have been measured with ultrafast four-wave-mixing (FWM) spectroscopy. They range from a few picoseconds (LL0) to a few hundred femtoseconds (LL1). The reaction time of the 2DEG is comparable to the period of its low energy collective excitations. The period of the lowest inter-LL MP collective modes [13,14] is $T_{MP} = 2\pi\hbar/\Omega_M$, where $\Omega_M \sim 15 - 20$ meV is the MP excitation energy, which is of the order of a few hundreds of femtoseconds. Thus, ~ 100 fs optical pulses provide access to the quantum kinetic regime of the QH system.

Among the different nonlinear optical techniques, femtosecond FWM spectroscopy is well suited for studying coherent dynamics [1,19]. It has been used to demonstrate that, in undoped semiconductor quantum wells (QW), this dynamics is dominated by Coulomb interactions [1,2,3,4,5,6,7]. Fluctuations beyond the Random Phase Approximation (RPA) generate a two-pulse FWM signal with a distinct time dependence [1,2]. In particular, the Pauli blocking (Phase Space Filling, PSF) effects [19] do not contribute during negative time delays, where exciton-exciton (X-X) interactions dominate in undoped QWs [1,2]. The time-dependent Hartree-Fock treatment of X-X interactions [3] predicts an *asymmetric* FWM temporal profile, with a negative time delay signal decaying twice as fast as the positive time delay signal [1,2,19]. The observation of strong deviations from this asymmetric temporal profile was interpreted as the signature of X-X correlations in undoped QWs [1,2].

Similar to undoped QWs, the interband absorption spectrum of a modulation doped QW subject to a perpendicular magnetic field is dominated by discrete LL peaks [20,21]. Despite some similarities however, there are large qualitative differences in the spectral and temporal profile of the nonlinear optical signal stemming from the different ways in which doped and undoped QWs respond to ultrafast excitation. In undoped QWs, the lowest electronic excitations are high energy interband transitions that react almost instantaneously to the presence of photoexcited carriers [22]. The ground state can then be considered as rigid, providing only the band structure and dielectric

screening. Consequently, Coulomb correlations only occur among *photoexcited* carriers. The role of such interactions can be analyzed by using theories such as the dynamics-controlled truncation scheme (DCTS) [5,6,23], the correlation expansion [7], or the Keldysh Green function technique [3,4]. In contrast, in doped QWs, the presence of a 2DEG leads to strong Coulomb correlations in the ground state itself, which result in long-range charge and spin order at sufficiently low temperatures and to collective electronic excitations. As a result, the DCTS assumptions break down [23]. The 2DEG can respond unadiabatically to the interactions with the photoexcited Xs by emitting low energy electronic excitations. One must distinguish such shake-up processes from those involving the nonequilibrium photoexcited electron gas. The differences in the physics of the doped and undoped systems manifest themselves strongly in the ultrafast nonlinear optical response.

The study of the ultrafast nonlinear optical dynamics of the QH system transcends across the boundaries of two communities largely disconnected up to now. Indeed, the transient optical properties of this system are governed by (i) the interband (X) excitations (with the 2DEG at rest), which consist of $1 e-h, 2 e-h, \dots$ pairs created in the LLs (studied by the nonlinear optics community), and (ii) the intraband 2DEG excitations (with unexcited QW and full valence band), e.g. the 1-MP, 2-MP, \dots and incoherent pair excitations (studied by the QH community). The ensemble of states that determine the nonlinear optical spectra to $(2\ell - 1)$ -th order in the optical field consist of products of up to $\ell e-h$ pairs and n 2DEG excitations. One can then draw an analogy with the X+phonon states that determine the ultrafast optical dynamics in undoped semiconductors [4,5,7,23]. However, there are some important differences. In the QH system, the 2DEG excitations are electronic in nature, and therefore subject to Pauli correlations with the photoexcited Xs, while the ground state electrons are strongly correlated. On the other hand, in the undoped system, the X operators commute with the collective excitation (phonon) operators, while the ground state correlations can be neglected. Thus the theoretical formulations used to study the nonlinear optical response in undoped semiconductors must be extended in order to treat correlations in the doped system.

Recent time-resolved FWM experiments probed for the first time the coherent regime of the 2DEG in a magnetic field and opened a new field of non-equilibrium Quantum Hall physics [20,21,24,25,26,27,28,29,30,31,32]. The purpose of this article is to review the recent developments in this emerging field. We first briefly discuss the linear absorption and two-pulse FWM experiments that probe the exciton dephasing. There are striking differences when compared to an undoped sample. The inter-LL MP excitations, which provide a dynamical coupling between the LL0 and LL1 excitons, are responsible for these differences. We then focus on recent three-pulse FWM experiments, which give access to two different time delays. The FWM signal along one of

these time delays probes the coherent inter-band dynamics of the QH system and reproduces the two-pulse FWM results. Measuring along the other time delay axis gives access to the intra-band dynamics of the QH system, which in the early coherent regime is governed by $X \leftrightarrow X + MP$, $X \leftrightarrow X$, and MP transient coherences. For short time delays along this new axis, the experiment reveals strong oscillations with a period given by the inverse LL0–LL1 energy splitting. For longer time delays, there is a slow rise of the three-pulse FWM signal on a timescale of several picoseconds, which only occurs for very low photoexcitation and is absent in the undoped QW. We also review a microscopic many-body theory that was developed in order to study the ultrafast coherent dynamics of strongly correlated systems and interpret the experiments. By comparing to this theory we identify the physical origin of the observed oscillations. The combined experimental and theoretical investigations reviewed here point out the important role of $X \leftrightarrow X + MP$ coherences and correlations, created by the nonlinear photoexcitation and the long range order of the QH system.

2 Experimental results

The experimental results discussed here were obtained by performing linear and non-linear optical measurements on a modulation doped QW, whose active region consisted of 10 periods of a 12 nm GaAs well and a 42 nm $Al_{0.3}Ga_{0.7}As$ barrier, the central 12 nm doped with Si. The sample was antireflection coated and mounted on sapphire windows for transmission measurements. The doped carrier density was $2.1 \times 10^{11} \text{ cm}^{-2}$ and the low temperature mobility $\sim 10^5 \text{ cm}^2/\text{Vs}$. The sample was kept in a magneto-optic cryostat at a temperature of $1.5 - 4^\circ\text{K}$. A perpendicular magnetic field ($B = 0 - 12 \text{ T}$) was applied along the growth direction of the QW. The measurements in the above doped system were compared to those in an undoped sample (without a 2DEG) with similar well and barrier sizes. The qualitative differences in the spectral and temporal profile of the linear and non-linear optical spectra of the two systems must thus be attributed to the 2DEG. In order to make the interpretation easier, σ_+ circularly polarized pulses were used. In this case, only one transition is allowed by the selection rules, which photoexcites spin- \downarrow electrons. In this section we discuss the experimental linear absorption and transient two- and three-pulse FWM spectra in the two systems.

2.1 Linear Absorption

We already see tell-tale signs of the important role of the cold 2DEG in the linear absorption spectrum [21]. Figs. 1 and 2 compare the σ_+ linear absorp-

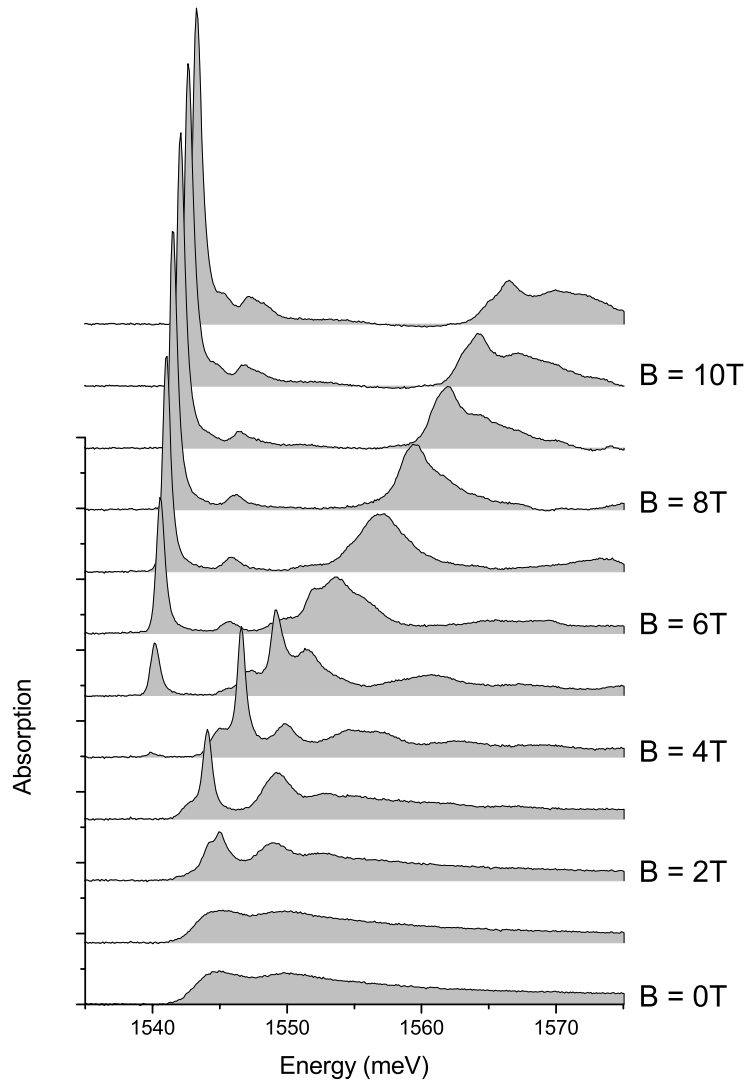


Fig. 1. σ_+ linear absorption of the doped QW for different magnetic fields. One sees absorption into the two lowest LLs. The onset of absorption into LL0 (at 4.3 T, $\nu = 2$) is accompanied by a sudden increase in the linewidth of the LL1 peak.

tion spectra of the modulation doped QW with those of the undoped QW for various magnetic fields. For both samples, one clearly sees the two peaks that are due to absorption into the two lowest LLs (LL0 and LL1). In the doped sample, LL0 absorption is only possible when the filling factor ν is smaller than two, in which case empty LL0 states are available ($B \geq 4.3$ T in Fig. 1). On the other hand, in the undoped QW, one observes a sharp LL0 peak down to small magnetic fields. The striking feature in the doped sample is the coincidence between a large increase in the linewidth of the LL1 peak and the onset of absorption into LL0. One sees no such increase in the LL1 linewidth in the undoped QW (Fig. 2). At the same time, the LL0 linewidth is not very

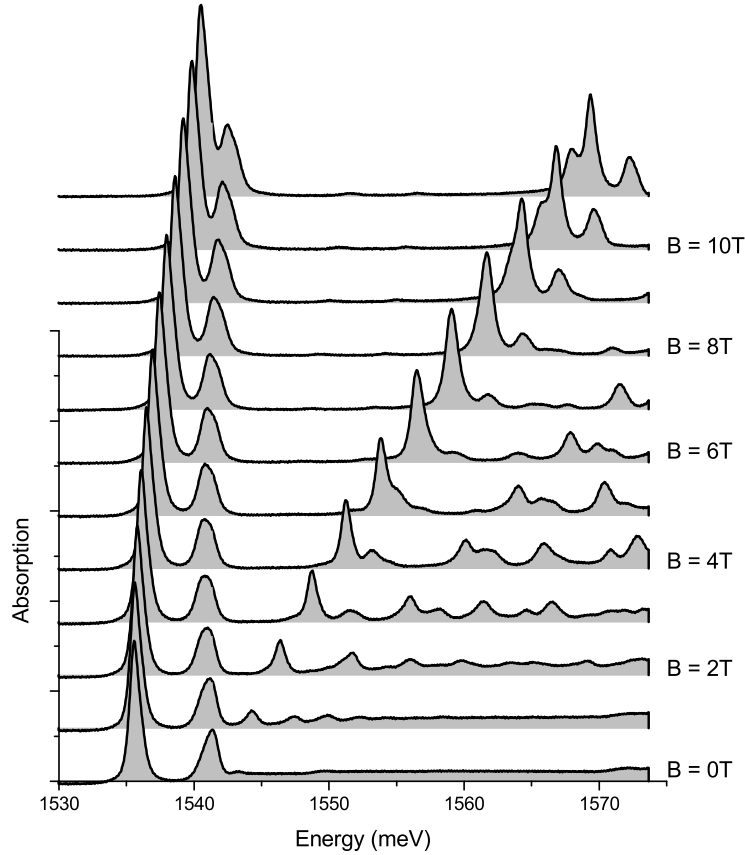


Fig. 2. σ_+ linear absorption for the undoped QW. There is no significant change in linewidth of the LL0 or LL1 peaks versus magnetic field.

sensitive to the filling factor ν . We conclude that the increased LL1 linewidth results from an increase in the dephasing rate of the LL1 magnetoexciton once empty LL0 states become available for scattering. For $\nu < 2$, one expects scattering of the LL1 magnetoexciton (X_1) into a LL0 magnetoexciton (X_0) accompanied by the emission (shake-up) of inter-LL MP excitations of the 2DEG. Noting that the LL0 \rightarrow LL1 magnetoplasmon is close in energy to the LL0-LL1 magnetoexciton splitting, we expect that this $X_1 \rightarrow X_0 +$ MP scattering process can be very efficient in limiting the lifetime of the LL1 exciton. In contrast, the LL0 exciton lifetime is not affected much by the inter-LL MPs since there are no states available for resonant scattering. The theoretical calculations discussed below confirm this scenario. The dynamics of the $X_1 \rightarrow X_0 +$ MP scattering process is studied here in full detail by looking at the spectral and temporal profiles of the two- and three-pulse FWM signals and by comparing between the doped and undoped QWs. The inter-LL MPs play a crucial role in the transient nonlinear optical response by providing a dynamical exciton coupling and by introducing different dynamics of the LL0 and LL1 excitons.

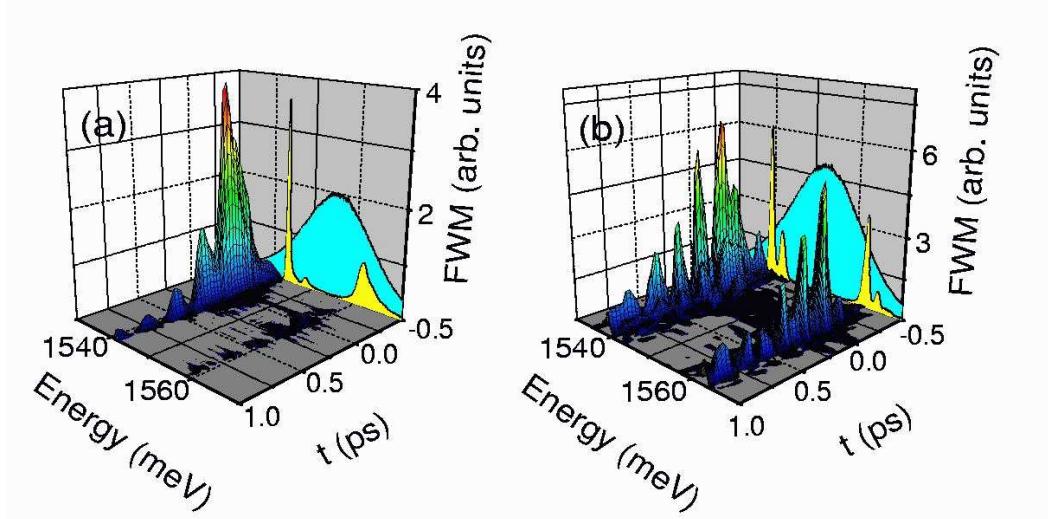


Fig. 3. Comparison of 2-pulse FWM transient spectra when the two LLs are equally excited for (a) doped QW and (b) undoped QW. The back panel shows the linear absorption and the pulse overlap with the two LL peaks.

2.2 Two-pulse FWM

In this section we discuss the two-pulse FWM experiments [20,21], where the QH sample is excited with two pulses propagating along directions \mathbf{k}_1 and \mathbf{k}_3 (named so for easier comparison with the three-pulse FWM experiments discussed in the next section). The FWM signal is measured in the direction $2\mathbf{k}_1 - \mathbf{k}_3$. We introduce a time delay Δt (or Δt_{13} for comparison with three-pulse FWM experiments) between the two pulses, where for negative delay pulse \mathbf{k}_1 comes first. Typically, the measurements were performed with weak photoexcitation intensity, keeping the total number of excited carriers under $2 \times 10^{10} \text{ cm}^{-2}$ or a tenth of the density of the 2DEG carriers. Only in this low excitation regime are the differences between the doped and undoped samples significant [21,31]. The FWM signal was spectrally resolved and the intensity measured as a function of wavelength (i.e. photon energy) as well as pulse time delay Δt_{13} . The spectral resolution allows one to separate out the contributions from the various LLs, which otherwise all contribute to the standard time-integrated FWM signal [19]. This spectral resolution and LL separation is important for identifying the physical mechanisms at work. Measurements under the same conditions were performed on the undoped samples for comparison. The important criterion for this comparison to be meaningful, given the differences in the linear absorption between the two systems, was to excite the same number of electron-hole pairs into each LL with a given laser pulse.

We start by discussing the case of photoexcitation of almost equal numbers of LL0 and LL1 carriers. Several unusual features are immediately apparent in the FWM signal from the doped QW, as compared to the FWM signal from

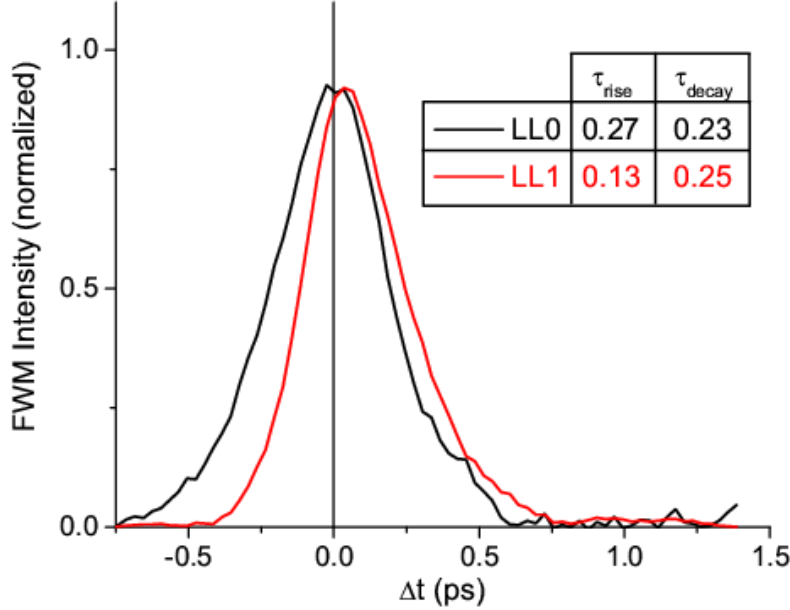


Fig. 4. Normalized 2-pulse FWM emission from LL0 and LL1 when the LL1 is preferentially excited over LL0 (60:1 ratio).

the similar undoped QW (see Fig. 3). The most striking is that, despite the equal excitation of both LLs, the doped QW shows a LL0 signal 35 times larger than the LL1 signal. In contrast, the undoped QW shows almost equal emission from both LLs, in proportion to the photoexcitation, as expected for a three-level system or RPA theory [19]. Importantly, although we see emission almost entirely from LL0, the doped QW FWM signal shows pronounced beats as a function of time delay Δt_{13} , with a period given by the inverse of the energy difference between the LL0 and LL1 absorption resonances. Strong beating for a single FWM resonance is a clear signal of non-Markovian dynamics. These beatings disappear in the case of LL1 photoexcitation discussed below. In contrast, the undoped QW shows beats from two emission peaks of similar strength, as expected for a three-level system or from RPA theory [19].

The picture is just as unusual when we tune the laser frequency to excite 60 times more carriers into LL1 than into LL0. Despite the extremely weak LL0 photoexcitation, the LL0 FWM signal in the doped QW is greatly enhanced: it is comparable to the LL1 signal despite the small PSF contribution at LL0. In contrast, in the undoped QW, there is almost no LL0 signal, as expected from the photoexcitation (60:1 for LL1:LL0). The large off-resonant LL0 signal in the doped system can come from LL1-LL0 coupling due to (i) X-X interactions, (ii) inter-LL X coherences, and (iii) inter-LL coherences assisted by the 2DEG excitations. The first two also contribute in the undoped QW, where however the LL0 signal is small. Therefore, these contributions are weak, and we conclude that the LL0-LL1 coupling mainly comes from an inter-LL coherence assisted by the 2DEG excitations.

In addition to the transfer of FWM strength to LL0, the doped QW signal shows a very unique dependence on Δt_{13} (Fig. 4). According to the RPA theory [33], the rise time of the $\Delta t_{13} < 0$ FWM signal should be 1/2 the decay time for $\Delta t_{13} > 0$ FWM, as measured in the undoped QW sample. This is also the measured result for the LL1 signal in the doped QW. Surprisingly however, the LL0 signal is almost symmetric as a function of Δt_{13} , with comparable signals for $\Delta t_{13} < 0$ and $\Delta t_{13} > 0$ (see Fig. 4). Such a large LL0 signal for $\Delta t_{13} < 0$ can only be a result of correlation effects beyond the RPA [1]. This doped QW effect is only seen for low photoexcitation intensity, which implies that the correlations are induced by the cold 2DEG.

2.3 Three-pulse FWM

In three pulse FWM, the sample was excited with three 100 fs, σ_+ pulses propagating along distinct directions \mathbf{k}_1 , \mathbf{k}_2 , and \mathbf{k}_3 . Pulses \mathbf{k}_1 and \mathbf{k}_2 (\mathbf{k}_3) are separated by a time delay Δt_{12} (Δt_{13}), where pulse \mathbf{k}_1 arrives first for negative values of the delay. The FWM signal is obtained in the background-free direction $\mathbf{k}_1 + \mathbf{k}_2 - \mathbf{k}_3$. Using an interference filter, we spectrally resolve the signal so as to separate out the contribution from each LL. We then measure the intensity from each LL as a function of the two above time delays. In particular, we measure along the Δt_{12} axis ($\Delta t_{13} = 0$) or the Δt_{13} axis ($\Delta t_{12} = 0$). Along the Δt_{13} axis, three-pulse FWM results describe the interband polarization dephasing similar to two-pulse FWM in the direction $2\mathbf{k}_1 - \mathbf{k}_3$. On the other hand, the three-pulse FWM signal along the Δt_{12} axis reflects the dynamics of intraband coherences, e.g. coherences between X and X or X and X+MP states, or between the ground state and the MP states. By comparing the FWM temporal profiles as function of Δt_{13} and Δt_{12} during subpicosecond time scales we arrive at a comprehensive picture of the dynamics of the interband and intraband coherences in the QH system.

The bulk of the three-pulse FWM measurements were performed at $B = 7$ T, which corresponds to $\nu = 1.3$ in this sample. Close to $\nu = 1$, the results did not depend strongly on the filling factor. The photo-excited carrier density ($5 \times 10^9 \text{ cm}^{-2}$) was typically much lower than the density of the doped 2DEG carriers. Here we only focus on the experiments for large excitation ratios of LL1 to LL0 (LL1:LL0 excitation ratio at least 10:1 in Fig. 5). The backpanel of Fig. 5 shows the overlap of the optical pulse with the LL0 and LL1 peaks in linear absorption. In this case of predominantly LL1 photoexcitation, the LL0 signal can only arise from correlation effects. Fig. 5a shows a large transfer of FWM signal strength from LL1 to LL0 in the doped QW, while Fig. 5b shows the FWM spectra for an undoped sample under similar excitation conditions for comparison. One does not see a large FWM signal from LL0 in the undoped QW, as expected for LL1 photoexcitation, while in the doped QW the

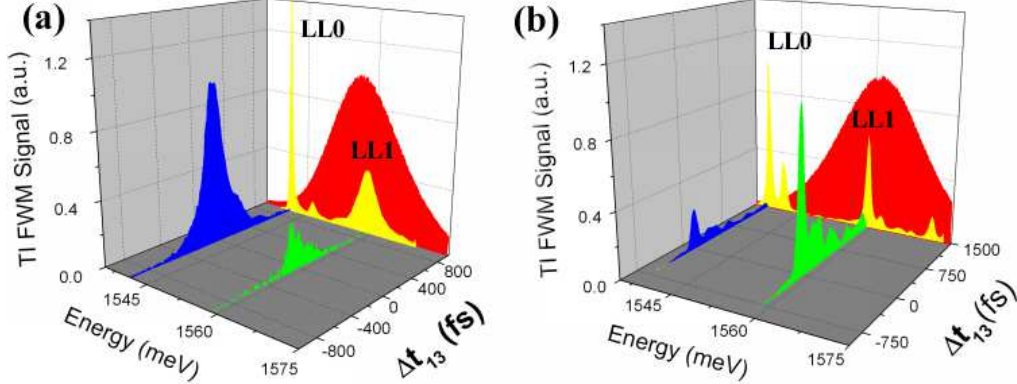


Fig. 5. Comparison of the (a) doped QW and (b) undoped QW FWM spectra along the Δt_{13} axis for LL1 photoexcitation. A temporally symmetric LL0 FWM signal dominates in the doped QW, while the LL1 FWM dominates in the undoped QW. The back panel shows the linear absorption and pulse overlap with the two peaks.

LL0 signal clearly dominates. We also see in Fig. 5a the unusually symmetric temporal profile of the LL0 signal, similar to two-pulse FWM.

We now turn our attention to the large off-resonant LL0 signal along the Δt_{12} axis. It is important to note that different time delays probe different physics in three-pulse FWM experiments. The measurements along the Δt_{12} axis provide new information about the dynamics of the intraband coherence that is not accessible with two-pulse FWM, while the Δt_{13} axis probes the interband coherence. For negative Δt_{12} , pulses \mathbf{k}_1 and \mathbf{k}_3 arrive together creating an intraband coherence, e.g. a $\text{X} \leftrightarrow \text{X} + \text{MP}$, $\text{X} \leftrightarrow \text{X}$, or MP coherence. For negative time delays, this coherence evolves for a time $|\Delta t_{12}|$, at which point it is probed by the arrival of pulse \mathbf{k}_2 . Thus, during early femtosecond time scales, the FWM signal versus Δt_{12} reflects the dynamics of the intraband coherence.

Fig. 6 shows the spectrally resolved FWM signal in the doped QW along the Δt_{12} axis for low photoexcitation and low temperature. We observe strong oscillations in the off-resonant signal at LL0 as function of Δt_{12} . There are only minor oscillations at LL1 or along the Δt_{13} axis. The oscillation frequency is comparable to the inter-LL energy spacing and increases linearly with the magnetic field. The decay rate of these oscillations is comparable to the sum of the LL0 and LL1 dephasing rates extracted from Fig. 5 (or Fig. 4) for both positive and negative Δt_{12} . With increasing photoexcitation intensity, the Δt_{12} oscillations disappear quickly, even before the decay of the overall FWM signal changes significantly. In contrast, along Δt_{13} , oscillations start to appear with increasing intensity in both the doped and the undoped QWs, which start to look alike as the photoexcited carriers dominate [21,31]. After presenting the theory used to describe the ultrafast nonlinear optical response, we will discuss the physical origin of the Δt_{12} oscillations and show that they are mainly due to the $\text{X} \leftrightarrow \text{X} + \text{MP}$ coherence.

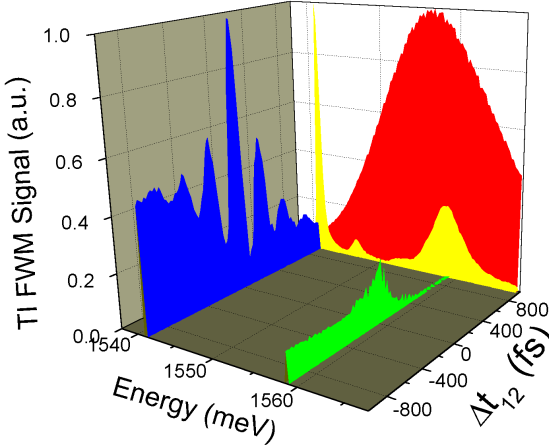


Fig. 6. FWM spectra along the Δt_{12} axis from the doped QW for large LL1/LL0 excitation. In the initial coherent regime, the LL0 signal displays strong oscillations.

3 Theory Overview

In this section we review the theoretical formulation of the ultrafast nonlinear optical response of the 2DEG [25,32]. We start with the standard two-band Hamiltonian H that describes conduction electron and valence hole discrete LLs coupled by the $e-e$, $e-h$, and $h-h$ Coulomb interactions [3]. The coupling of the optical field is treated within the dipole approximation and induces interband transitions characterized by the Rabi energy $d(t) = \mu E(t)\sqrt{N}$, where $E(t)$ is the optical pulse, μ is the interband dipole transition matrix element, and N is the LL degeneracy (we set $\hbar = 1$ from now on). Similar to the experiment, we consider right-circularly polarized optical pulses (σ_+), which excite only spin- \downarrow electrons due to the selection rules. For low photoexcitation intensity, the QH system is probed in a perturbative fashion, which allows for the observation of the 2DEG correlations. In this excitation regime, one can expand in powers of the optical field and describe the FWM signal by calculating the third-order nonlinear polarization.

3.1 Polarization and Population Equations of Motion

The ultrafast nonlinear optical response of the QH system is dominated by the interactions among its collective excitations: the interband excitons and the intraband magnetoplasmons. The LL_n electron- LL_m hole magnetoexcitons with total momentum \mathbf{q} are created by the collective interband operators $\hat{X}_{\mathbf{q}nm}^\dagger$ defined in Ref. [32]. The dipole optical transitions excite the LL_n magnetoexciton states $|X_n\rangle = \hat{X}_n^\dagger |G\rangle$, where $\hat{X}_n = \hat{X}_{nn0}^\dagger$, whose difference from undoped semiconductors is that the exciton operator now acts on the strongly

correlated ground eigenstate, $|G\rangle$, of the many-body Hamiltonian H . For the small momenta relevant to optics experiments, the 2DEG intraband excitation spectrum is dominated by the collective MP modes. A $LLm \rightarrow LLn$ MP may be thought of as a pair formed by an electron in LLn and a hole in the electron LLm 2DEG created by the collective density operator $\hat{\rho}_{\mathbf{q}nm\sigma}^e$ [13,14,32,34,35]. It is convenient to also introduce a similar operator $\hat{\rho}_{\mathbf{q}nm\sigma}^h$ for the valence band hole states [32]. The photoexcited LL0 and LL1 optical transitions are dynamically coupled by the $LL0 \rightarrow LL1$ inter-LL MPs.

Unlike in linear optics or Raman/inelastic light scattering experiments, the ultrafast FWM signal is generated by interactions and correlations involving the elementary excitations of the system. The main challenge facing the calculation is the description of the interaction-induced quantum dynamics during time scales shorter than the dephasing and relaxation times. The interactions with the ground state 2DEG couple the exciton states to the X+2DEG* states $|Y_n\rangle = \hat{Y}_n^\dagger|G\rangle$, where 2DEG* denotes an excited 2DEG configuration. These states are defined as follows after requiring that $\langle X_m|Y_n\rangle = 0$:

$$H|X_n\rangle = \Omega_n|X_n\rangle - (1 - \nu_n) \sum_{n' \neq n} V_{nn'}|X_{n'}\rangle + |Y_n\rangle. \quad (1)$$

Ω_n is the X_n energy, $V_{nn'}$ gives the static Coulomb-induced coupling of the different LL Xs, and ν_n is the ground state filling factor of the LLn spin- \downarrow electron states. The operator

$$\hat{Y}_n = [\hat{X}_n, H] - \Omega_n \hat{X}_n + (1 - \nu_n) \sum_{n' \neq n} V_{nn'} \hat{X}_{n'}, \quad (2)$$

then describes the interactions between X_n and all the other carriers in the system (i.e. X-X, X-MP, and X-2DEG interactions). By retaining for simplicity the contributions from the photoexcited LLs (LL0 and LL1), we can express \hat{Y}_n as a linear combination of the operators $\hat{X}_{\mathbf{q}01}\hat{\rho}_{\mathbf{q}nm}^{e,h}$ and $\hat{X}_{\mathbf{q}10}\hat{\rho}_{\mathbf{q}nm}^{e,h}$ and obtain the property $\hat{Y} = \hat{Y}_1 = -\hat{Y}_0$ [32].

The optical signal is determined by the LLn optical polarizations $P_n = \langle \hat{X}_n \rangle$, which satisfy the equations of motion [32]

$$i\partial_t P_n = \Omega_n P_n - (1 - \nu_n) \sum_{n' \neq n} V_{nn'} P_{n'} - d(t)[1 - \nu_n - \Delta\nu_n] + \langle \hat{Y}_n \rangle, \quad (3)$$

where the interband density matrix $\langle \hat{Y}_n \rangle$ gives the interaction-induced contribution that distinguishes semiconductors from atomic few level systems and determines the unusual off-resonant LL0 signal in the doped QW. $\Delta\nu_n$ is the change in the LLn filling factor induced by the photoexcitation and determines

the Pauli Blocking (PSF) contribution to the nonlinear polarization P_n (third term on the rhs of Eq.(3)):

$$i\partial_t\Delta\nu_n = 2[d^*(t)P_n - d(t)P_n^*]/N + \langle[\hat{Y}_n, \hat{X}_n^\dagger]\rangle^* - \langle[\hat{Y}_n, \hat{X}_n^\dagger]\rangle. \quad (4)$$

To describe dephasing and relaxation due to degrees of freedom not included in the Hamiltonian H , we also introduce the X dephasing rates Γ_n and the population relaxation times T_1 .

The intraband density matrix $\langle[\hat{Y}_n, \hat{X}_n^\dagger]\rangle$ describes the redistribution of the photoexcited exciton populations due to the interactions and can be expressed as a linear combination of the density matrices $\langle\hat{X}^\dagger\hat{X}\rangle$, $\langle\hat{\rho}_\sigma^e\hat{\rho}_\downarrow^e\rangle$, $\langle\hat{\rho}_\sigma^e\hat{\rho}_\downarrow^h\rangle$, and $\langle\hat{\rho}_\downarrow^h\hat{\rho}_\downarrow^h\rangle$ [32]. In the undoped system, one can show that the only independent intraband density matrices that contribute to the third order nonlinear polarization have the form $\langle\hat{X}^\dagger\hat{X}\rangle$ [32]. These describe exciton populations as well as X↔X coherences. In the doped system, the *ground state* electrons give an additional contribution to the third order polarization determined by the intraband density matrices $\langle\hat{\rho}^e\hat{X}^\dagger\hat{X}\rangle$, which in the undoped system contribute to fifth order or higher. These density matrices describe the coherent coupling between the X and X+MP states, i.e. X↔X+MP many-particle coherences induced by the correlations of the QH system.

The main effects in the doped system can be described by calculating the interaction-induced density matrices $\langle[\hat{Y}_n, \hat{X}_n^\dagger]\rangle$ and $\langle\hat{Y}_n\rangle$ up to third order in the optical fields. For this we first decompose these density matrices into correlated and uncorrelated parts, which allows us to isolate the contributions due to the correlations and devise appropriate approximations. Although in the undoped system this can be achieved by introducing cumulants (the basis of the DCTS [23]), in the doped system the ground state correlations as well as correlations between the photoexcited Xs and the 2DEG elementary excitations must also be taken into account. The DCTS assumptions and Wick's theorem break down in the case of the correlated 2DEG, so new schemes must be devised. To motivate a density matrix decomposition that reduces to the DCTS in the case of undoped semiconductors but also applies to systems with strongly correlated ground states, we first decompose the photoexcited many-body state $|\psi(t)\rangle$ that evolves from the ground state $|G\rangle$ into interacting and noninteracting parts as discussed in the next section.

3.2 Decomposition of the photoexcited states

We note that, since the Hamiltonian H conserves the number of valence band holes, there is a one to one correspondence between the number of holes created (annihilated) and the number of photons absorbed (emitted). We can therefore

classify the photoexcited states in terms of the number of photoexcited holes: $|\psi\rangle = |\psi_0\rangle + |\psi_1\rangle + |\psi_2\rangle + \dots$, where $|\psi_n\rangle$ is the *collective* n - h photoexcited state [25]. States with $n \geq 3$ do not contribute to the third-order polarization.

The linear response is described by the time evolution of the 1- h many-body state $|\psi_{1L}\rangle$ calculated to first order in the optical field. We decompose this 1- h state into X and interacting X+2DEG* contributions:

$$|\psi_{1L}\rangle = \sum_n \frac{P_n^L}{1 - \nu_n} |X_n\rangle + |\bar{\psi}_{1L}\rangle, \quad (5)$$

where we require that $\langle X_n | \bar{\psi}_{1L} \rangle = 0$. The X amplitude $P_n^L = \langle X_n | \psi_{1L} \rangle$ coincides with the linear polarization, while, to first order in the optical field, $\langle \hat{Y}_n \rangle = \langle Y_n | \bar{\psi}_{1L} \rangle$. The dephasing of the linear polarization is therefore determined by the time evolution of the X+2DEG* states $|Y_n\rangle$. These states can be expanded in a basis of states $|Y_\alpha\rangle$, such as the orthonormal Lanczos states introduced in Refs. [25,32] or the continuum of X+MP states $\hat{X}_{\mathbf{q}01}^\dagger \hat{\rho}_{-\mathbf{q}nm}^e |G\rangle$ and $\hat{X}_{\mathbf{q}10}^\dagger \hat{\rho}_{-\mathbf{q}nm}^e |G\rangle$ for all values of the momentum \mathbf{q} that contribute to $|Y\rangle$ [32]. Retaining the above X+MP states corresponds to treating the correlations between the X and a MP nonperturbatively, in a way analogous to the treatment of the carrier-magnon three-body correlations in the case of the Hubbard [36] or double exchange [37] Hamiltonians, which in 1D agreed well with exact results. An analogous treatment of three-body correlations between Xs and Fermi sea excitations was used to treat the Fermi Edge Singularity [8,38].

To obtain the equation of motion for the linear X+MP amplitudes $\langle Y_\alpha | \bar{\psi}_{1L} \rangle$, we first consider the action of the Hamiltonian H on $|Y_\alpha\rangle$ and define the state $|Z_\alpha\rangle$ by requiring that it is orthogonal to both $|Y_\alpha\rangle$ and all $|X_n\rangle$ [25,32]:

$$H|Y_\alpha\rangle = \bar{\Omega}_\alpha |Y_\alpha\rangle + \sum_n W_{\alpha n} |X_n\rangle + |Z_\alpha\rangle, \quad (6)$$

where $\bar{\Omega}_\alpha$ is the energy of the state $|Y_\alpha\rangle$, $W_{\alpha n}$ gives the interaction-induced coupling between $|Y_\alpha\rangle$ and $|X_n\rangle$, and $|Z_\alpha\rangle$ comes from the scattering between the X and the MP. We thus obtain the equation of motion [25,32]

$$i\partial_t \langle Y_\alpha | \bar{\psi}_{1L} \rangle = (\bar{\Omega}_\alpha - i\gamma_\alpha) \langle Y_\alpha | \bar{\psi}_{1L} \rangle + \sum_n W_{\alpha n}^* P_n^L + \langle Z_\alpha | \bar{\psi}_{1L} \rangle, \quad (7)$$

whose solution has the form $\langle Y_\alpha | \bar{\psi}_{1L} \rangle = \sum_n W_{\alpha n}^* \int_{-\infty}^t K_\alpha(t - t') P_n^L(t') dt'$. The X+MP correlation function $K_\alpha(t) = -i \langle Y_\alpha | e^{-i\bar{H}t} | Y \rangle$ describes memory effects governed by noninstantaneous X+MP interactions, where \bar{H} is the Hamiltonian H projected within the subspace of X+2DEG* states. The semiclassical

approximation corresponds to approximating $K_\alpha(t) \sim iT_2^{-1}\delta(t)$, where T_2 is the exciton dephasing time. However, memory effects described by the time dependence of $K(t)$ are important for determining the LL1 exciton linewidth for $\nu < 2$ (Fig. 1) [21,25,32].

The 2- h and 0- h many-body states $|\psi_2\rangle$ and $|\psi_0\rangle$ are photoexcited via two-photon nonlinear processes. The first photon excites a 1- h state, $|X_n\rangle$ or $|\bar{\psi}_{1L}\rangle$, from the ground state. The second photon then excites ($|\psi_2\rangle$) or deexcites ($|\psi_0\rangle$) a second $e-h$ pair. This second transition may or may not be accompanied by interactions with the carriers in the 1- h states already excited by the first transition. We separate out the above interacting and noninteracting contributions to second order in the optical field as follows:

$$|\psi_2\rangle = \frac{1}{2} \sum_{nm} \frac{P_n^L P_m^L}{(1-\nu_n)(1-\nu_m)} \hat{X}_n^\dagger |X_m\rangle + \sum_n \frac{P_n^L}{1-\nu_n} \hat{X}_n^\dagger |\bar{\psi}_{1L}\rangle + |\bar{\psi}_2\rangle, \quad (8)$$

where $|\bar{\psi}_2\rangle$ describes the correlated X-X and X-X+2DEG* contributions, and

$$|\psi_0\rangle = \langle G|\psi\rangle |G\rangle - \sum_n \frac{P_n^{L*}}{1-\nu_n} \hat{X}_n |\bar{\psi}_{1L}\rangle + |\bar{\psi}_0\rangle, \quad (9)$$

where $|\bar{\psi}_0\rangle$ is the 2DEG* state created by the Raman process of excitation and then de-excitation of an $e-h$ pair assisted by correlations with the 2DEG.

3.3 Density matrix decompositions

By substituting the above decomposition of the photoexcited states, one arrives at the following decomposition of the density matrix $\langle \hat{M} \rangle$, where the operator \hat{M} , $\langle G|\hat{M}|G\rangle = 0$, connects states with the same number of holes:

$$\begin{aligned} \langle \hat{M} \rangle = & \langle \hat{M} \rangle_c + \sum_n \frac{P_n^{L*}}{1-\nu_n} \langle G|[\hat{X}_n, \hat{M}]|\bar{\psi}_{1L}\rangle + \sum_n \frac{P_n^L}{1-\nu_n} \langle \bar{\psi}_{1L}|[\hat{M}, \hat{X}_n^\dagger]|G\rangle \\ & + \sum_{nm} \frac{P_n^{L*} P_m^L}{(1-\nu_n)(1-\nu_m)} \langle X_n|\hat{M}|X_m\rangle + O(E^4), \end{aligned} \quad (10)$$

where the correlated contribution $\langle \hat{M} \rangle_c$ is determined by its equation of motion as discussed in Ref. [32]. The rest of the terms in Eq.(10) are given by products of 1- h state amplitudes, X or X+2DEG*, and arise from uncorrelated interband transitions. The time evolution of these product terms is determined by the X and X+2DEG* dephasing. In contrast, the dephasing of the correlated contribution $\langle \hat{M} \rangle_c$ is determined by the intraband dynamics, which introduces new time scales that affect the evolution of the transient FWM signal.

In the undoped system, the ultrafast dynamics is solely determined by the X states, whose coherent coupling is described by the equation of motion [32]

$$i\partial_t \langle |X_m\rangle \langle X_n| \rangle_c = (\Omega_n - \Omega_m - i\gamma_{nm}) \langle |X_m\rangle \langle X_n| \rangle_c + (1 - \nu_m) \sum_{m' \neq m} V_{m'm} \langle |X_{m'}\rangle \langle X_n| \rangle_c - (1 - \nu_n) \sum_{n' \neq n} V_{nn'} \langle |X_m\rangle \langle X_{n'}| \rangle_c + i P_n^L P_m^{L*} (\Gamma_n + \Gamma_m - \gamma_{nm}) + \langle |X_m\rangle \langle Y_n| \rangle_c - \langle |X_n\rangle \langle Y_m| \rangle_c^*, \quad (11)$$

As can be seen from the above equation, incoherent exciton populations ($n = m$) or X↔X coherences ($n \neq m$) can be photoexcited due to (i) the difference between the intraband relaxation rate γ_{nm} and the sum of the exciton dephasing rates $\Gamma_n + \Gamma_m$, and (ii) the coupling between the X and X+MP states described by the last two terms on the rhs. The former is the only source in the undoped system, while the latter X↔X+MP coupling dominates in the doped system and is described by the equation of motion [32]

$$i\partial_t \langle |X_m\rangle \langle Y_\alpha| \rangle_c = \left(\bar{\Omega}_\alpha - \Omega_m - i\Gamma_{\alpha m} \right) \langle |X_m\rangle \langle Y_\alpha| \rangle_c + \sum_{n'} W_{\alpha n'}^* \langle |X_m\rangle \langle X_{n'}| \rangle_c + (1 - \nu_m) \sum_{m' \neq m} V_{m'm} \langle |X_{m'}\rangle \langle Y_\alpha| \rangle_c + i (\Gamma_m + \gamma_\alpha - \Gamma_{\alpha m}) P_m^{L*} \langle Y_\alpha | \bar{\psi}_{1L} \rangle + \langle |X_m\rangle \langle Z_\alpha| \rangle_c - \left[\langle |Y_m\rangle \langle Y_\alpha| \rangle_c - \langle \bar{\psi}_{1L} | Y_m \rangle \langle Y_\alpha | \bar{\psi}_{1L} \rangle \right]. \quad (12)$$

The separation of the photoexcited states into interacting and noninteracting arts also suggests the following decomposition of the interband density matrix:

$$\langle \hat{Y} \rangle = \sum_n \frac{P_n^{L*}}{1 - \nu_n} \langle G | [\hat{X}_n, \hat{Y}] | \psi_2 \rangle + \sum_n \frac{P_n^L}{1 - \nu_n} \langle [\hat{Y}, \hat{X}_n^\dagger] \rangle_c + \frac{1}{2} \sum_{nm} \frac{P_n^L P_m^L}{(1 - \nu_n)(1 - \nu_m)} \langle \bar{\psi}_{1L} | [[\hat{Y}, \hat{X}_n^\dagger], \hat{X}_m^\dagger] | G \rangle + \langle \hat{Y} \rangle_c, \quad (13)$$

where the correlated part $\langle \hat{Y} \rangle_c$ is determined by the dynamics of the states $|Y\rangle$ and $|\bar{\psi}_0\rangle$, and by the coupling between $|\bar{\psi}_1\rangle$ and $|\bar{\psi}_2\rangle$ (exciton–biexciton transition amplitude in undoped semiconductors [23]). The first term on the rhs of Eq.(13) describes the coherent X–X interaction contribution, determined by the dynamics of the 2–h state $[\hat{Y}^\dagger, \hat{X}_n^\dagger] |G\rangle$ which is a linear combination of two-exciton states [25,32]. In the undoped system, the above 2–h amplitude can be expressed in terms of the X–X correlation function discussed in Ref. [39], which is analogous to the X–MP correlation function $K_\alpha(t)$ discussed above. The rest of the terms on the rhs of Eq.(13) are due to the scattering of the polarization P_n^L off incoherent populations and intraband coherences, such as the X↔X and X↔X+MP coherences discussed above. Noting the huge difference in the LL0 signal between the doped and undoped QWs, we conclude

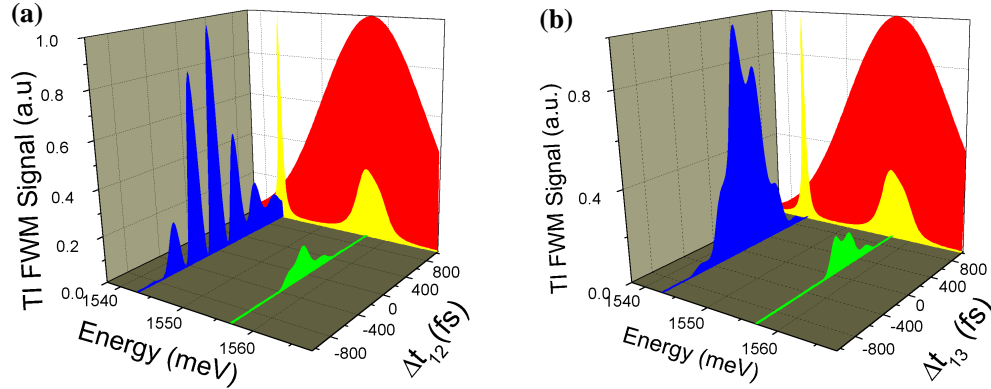


Fig. 7. Calculation of the FWM Signal in the doped QW along (a) the Δt_{12} axis (b) the Δt_{13} axis. Back panel: linear absorption spectrum and optical pulse.

that the contribution due to the $X \leftrightarrow X + MP$ coherences dominates the ultrafast nonlinear optical response of the 2DEG in the femtosecond regime. In the next section we present a model calculation based on the above microscopic theory that captures the main experimental features.

4 Comparison between theory and experiment

In this section we discuss the results of our numerical calculation of the transient three-pulse FWM spectrum at $\nu = 1$. These were obtained as above after retaining the states $|X_n\rangle$, $n = 0, 1$, and $|Y\rangle$ and treating for simplicity the effects of the rest of the basis states by introducing dephasing rates [25,32]. The independent parameters that enter this model calculation were estimated by comparing to the experimental linear absorption [21,25,32]; our conclusions are not sensitive to their precise values. Here we consider the ideal 2D system, where the coherent MP contribution discussed in Refs. [25,32] vanishes.

Fig. 7 shows the calculated transient FWM for LL1 photoexcitation, while the back panel shows the calculated linear absorption. These results reproduce the qualitative temporal and spectral features observed in the experiment within the femtosecond coherent regime, as function of energy, the two time delays, and the central photoexcitation frequency. The main contribution to the calculated FWM signal comes from the $X_n \rightarrow X_{01} + MP$ coherences $M_n = \langle |X_n\rangle \langle Y| \rangle_c$. This can be seen in Fig. 8, which compares to the calculation with $M_n = 0$. In the latter case, the FWM signal is determined by PSF and X-X contributions analogous to the undoped system, which, similar to the experiment, give a small LL0 signal. The $X \leftrightarrow X + MP$ coherences can be photoexcited either by pulses 1 and 3 (M_n^{13}) or by pulses 2 and 3 (M_n^{23}). M_0 (M_1) comes from the scattering of the LL0 valence hole (LL1 conduction electron) to LL1 (LL0) accompanied by the emission of an inter-LL MP.

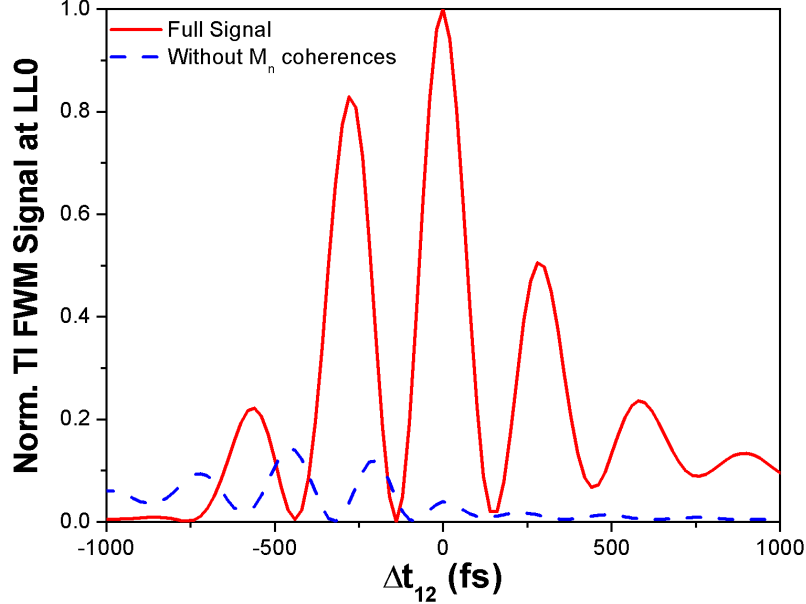


Fig. 8. Comparison of the calculated LL0 FWM signal along the Δt_{12} axis (solid line) with the signal calculated by setting $M_n = 0$ (dashed line).

The main contribution to the Δt_{12} oscillations of the FWM signal comes from the interference between the two nonlinear processes described schematically in Fig. 9. Pulses \mathbf{k}_1 and \mathbf{k}_3 arrive simultaneously in the sample to create a density of excitons in LL1. These excitons scatter into LL0 with the excitation of a MP, thereby creating the coherence M_1^{13} . This coherence then evolves for a time $|\Delta t_{12}|$ accumulating negligible phase due to the small M_1 energy. It is then probed by a P_0 polarization created by \mathbf{k}_2 , resulting in a FWM signal in $\mathbf{k}_1 + \mathbf{k}_2 - \mathbf{k}_3$ (Fig. 9a). Due to the symmetry of \mathbf{k}_1 and \mathbf{k}_2 in the $\mathbf{k}_1 + \mathbf{k}_2 - \mathbf{k}_3$ signal, we also have a process where \mathbf{k}_2 and \mathbf{k}_3 create the coherence M_1 (i.e. M_1^{23}), which is then probed by \mathbf{k}_1 . However, one must keep track of the time delays. As shown in Fig. 9b, \mathbf{k}_1 and \mathbf{k}_3 arrive together and contribute a LL1 polarization (\mathbf{k}_3) and a LL0 polarization (\mathbf{k}_1). These polarizations evolve in the sample for a time $|\Delta t_{12}|$ and accumulate a phase of $(\Omega_0 - \Omega_1)\Delta t_{12}$, where Ω_n denotes the energy of X_n . Pulse \mathbf{k}_2 then contributes a LL1 polarization that creates the M_1^{23} coherence with the decaying LL1 polarization from \mathbf{k}_3 . M_1^{23} is instantaneously probed by the decaying LL0 polarization created earlier by \mathbf{k}_1 , which results in a FWM signal with the accumulated phase $(\Omega_0 - \Omega_1)\Delta t_{12}$. The above contributions from M_1^{13} and M_1^{23} will interfere with each other for $|\Delta t_{12}|$ within the decay times of the polarizations, which results in the strong oscillations at the inter-LL frequency $\Omega_1 - \Omega_0$ along the Δt_{12} axis observed in the experiment. At the same time, the symmetric temporal profile along the Δt_{13} axis of the LL0 FWM signal due to M_n results from the much larger LL1 polarization dephasing as compared to the LL0 polarization dephasing, due to the $X_1 \rightarrow X_{01} + MP$ scattering process.

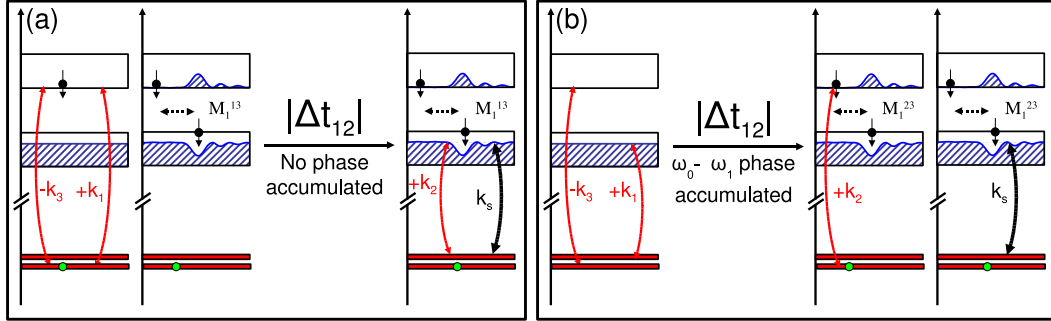


Fig. 9. Third-order process that describes the main contribution to the FWM signal due to (a) M_1^{13} (b) M_1^{23} .

5 Conclusions

In conclusion, we discussed recent ultrafast two- and three-pulse FWM results that demonstrate the important role of *non-instantaneous* correlations between photoexcited excitons and the inter-LL collective excitations of the 2DEG. We showed that three-pulse transient FWM spectroscopy can be used to access simultaneously the intra- and inter-band coherent dynamics of the QH system. Even for very small excitation of the LL0 transition, the FWM signal in the doped system is dominated by a large off-resonant peak at the LL0 energy with strong coherent oscillations and symmetric temporal profile. Using a microscopic many-body theory we showed that this signal is due to many-particle coherences created via the non-instantaneous interactions of photoexcited carriers and MPs. In particular, the noninstantaneous $X_1 \rightarrow X_{01} + \text{MP}$ interaction process both creates an intraband coherence and leads to strong LL1 exciton dephasing. Such effects govern the LL0 FWM temporal and spectral profiles. We showed for example that strong temporal oscillations result from the interference of different FWM contributions of the above intraband coherences. The combination of ultrafast nonlinear spectroscopy and QH physics initiates a new field of QH dynamics. Future experimental and theoretical activity in this area will further progress our understanding and manipulation of non-equilibrium correlations and quantum coherent phenomena in nanostructures.

This work was supported by the EU Research Training Network HYTEC (HPRN-CT-2002-00315) and by the U.S. Department of Energy under Contract No. DE-AC03-76SF00098. Part of this work was performed in collaboration with N. Fromer and A. T. Karathanos.

References

[1] D. S. Chemla and J. Shah, *Nature* **411** 549 (2001).

- [2] D. S. Chemla, *Nonlinear Optics in Semiconductors*, edited by R. K. Willardson and A. C. Beers (Academic Press, 1999).
- [3] W. Schäfer and M. Wegener, *Semiconductor optics and transport phenomena* (Springer, Berlin, 2002).
- [4] H. Haug and A.-P. Jauho, *Quantum Kinetics in Transport and Optics of Semiconductors* (Springer, Heidelberg, 1996).
- [5] V. M. Axt and S. Mukamel, Rev. Mod. Phys. **70**, 145 (1998).
- [6] V. M. Axt and T. Kuhn, Rep. Prog. Phys. **67**, 433 (2004).
- [7] F. Rossi and T. Kuhn, Rev. Mod. Phys. **74**, 895 (2002).
- [8] I. E. Perakis and T. V. Shahbazyan, Surf. Sci. Rep. **40**, 1 (2000); Int. J. Mod. Phys. B **13**, 869 (1999); I. E. Perakis, Chem Phys. **210**, 259 (1996); T. V. Shahbazyan, N. Primozich, and I. E. Perakis, Phys. Rev. B **62**, 15925 (2000).
- [9] H. A. Fertig and G. Murthy, Phys. Rev. Lett. **95** 156802 (2005).
- [10] K. J. Boller, A. Imamoglu and S. E. Harris, Phys. Rev. Lett. **66**, 2593 (1991).
- [11] A. S. Zibrov *et al.*, Phys. Rev. Lett. **75** 001499 (1995).
- [12] M. E. Donovan *et al.*, Phys. Rev. Lett. **87**, 237402 (2001); K. B. Ferrio and D. G. Steel, Phys. Rev. Lett. **80**, 786 (1998); G. Bartels *et. al.*, Phys. Rev. B **55**, 16404 (1997).
- [13] T. Chakraborty and P. Pietiläinen, *The Quantum Hall Effects, Fractional and Integral*, second edition (Springer, Berlin, Heidelberg, New York, 1995).
- [14] D. Yoshioka, *The Quantum Hall Effect*, (Springer-Verlag, 2002).
- [15] H. L. Stormer, D. C. Tsui, and A. C. Gossard, Rev. Mod. Phys. **71**, S298 (1999).
- [16] *Perspectives in Quantum Hall Effects*, S. Das Sarma and A. Pinczuk (eds.), (Wiley, New York, 1977).
- [17] A. Pinczuk *et. al.*, Phys. Rev. Lett. **61**, 2701 (1988); *ibid* **70**, 3983 (1993); C.F. Hirjibehedin *et. al.* Phys. Rev. Lett. **95**, 066803 (2005).
- [18] J. P. Eisenstein, Solid State Commun. **117**, 123 (2001).
- [19] J. Shah, *Ultrafast spectroscopy of semiconductors and semiconductor nanostructures* (Springer, Berlin, New York, 1999).
- [20] N. A. Fromer, C. E. Lai, D. S. Chemla, I. E. Perakis, D. Driscoll, and A. C. Gossard, Phys. Rev. Lett. **89**, 067401 (2002).
- [21] N. A. Fromer, C. Schüller, C. E. Lai, D. S. Chemla, I. E. Perakis, D. Driscoll, and A. C. Gossard, Phys. Rev. B **66**, 205314 (2002).
- [22] S. Louie in *Computational Materials Sciences*, edited by C. Y. Fong (World Scientific, Singapore, 1998); L. J. Sham, Phys. Rev. **150**, 720 (1966).

- [23] V. M. Axt and A. Stahl, *Z. Phys. B* **93**, 195 (1994); V. M. Axt, K. Victor, and A. Stahl, *Phys. Rev. B* **53**, 7244 (1996); V. M. Axt, K. Victor, and A. Stahl, *Phys. Rev. B* **53**, 7244 (1996).
- [24] N. A. Fromer, C. Schüller, D. S. Chemla, T. V. Shahbazyian, I. E. Perakis, K. Maranowski, and A. C. Gossard, *Phys Rev. Lett.* **83**, 4646 (1999).
- [25] A. T. Karathanos, I. E. Perakis, N. A. Fromer, and D. S. Chemla, *Phys. Rev. B* **67**, 035316 (2003).
- [26] I. E. Perakis, *Phys. Stat. Sol. B* **238**, 502 (2003).
- [27] I. E. Perakis and D. S. Chemla, *Solid State Commun.* **127**, 147 (2003).
- [28] I. E. Perakis and D. S. Chemla, *Phys. Stat. Sol. B* **234**, 242 (2003).
- [29] C. Schueller, I. E. Perakis, N. A. Fromer, and D. S. Chemla, in *Nonequilibrium Physics at Short Time Scales: Formation of Correlations*, ed. by Klaus Morawetz, 209 (Springer Berlin, Heidelberg, New York, 2004).
- [30] N. A. Fromer, C. Schüller, D. S. Chemla, T. V. Shahbazyian, I. E. Perakis, D. Driscoll, and A. C. Gossard, *Physica E* **12**, 550 (2002).
- [31] K. M. Dani, J. Tignon, M. Breit, D. S. Chemla, E. G. Kavousanaki, A. T. Karathanos, and I. E. Perakis, *Phys. Rev. Lett.* (submitted).
- [32] I. E. Perakis and E. G. Kavousanaki, *Chem. Phys.* **318**, 118 (2005).
- [33] M. Wegener, D. S. Chemla, S. Schmitt–Rink, and W. Schäfer, *Phys. Rev. A* **42**, 5675 (1990).
- [34] A. H. MacDonald, H. C. A. Oji and S. M. Girvin, *Phys. Rev. Lett.* **55**, 2208 (1985); H. C. A. Oji and A. H. MacDonald, *Phys. Rev. B* **33**, 3810 (1986).
- [35] C. Kallin and B. I. Halperin, *Phys. Rev. B* **30**, 5655 (1984).
- [36] J. Igarashi, M. Takahashi, and T. Nagao, *J. Phys. Soc. Jpn* **68**, 3682 (1999); J. Igarashi, *J. Phys. Soc. Jpn* **54**, 260 (1985).
- [37] M. D. Kapetanakis, A. Manousaki, and I. E. Perakis, cond-mat/0601025; *Phys. Rev. B* (submitted).
- [38] A. E. Ruckenstein and S. Schmitt–Rink, *Phys. Rev. B* **35**, 7551 (1987); A. E. Ruckenstein and S. Schmitt–Rink, *Int. J. Mod. Phys. B* **3**, 1809 (1989); I. E. Perakis and Y.–C. Chang, *Phys. Rev. B* **47**, 6573 (1993); J. F. Mueller, A. E. Ruckenstein, and S. Schmitt–Rink, *Phys. Rev. B* **45**, 8902 (1992).
- [39] Th. Östreich, K. Schönhammer, and L. J. Sham, *Phys. Rev. B* **58**, 12920 (1998).